Desalination and Water Treatment
www.deswater.com

doi: 10.5004/dwt.2019.24735

169 (2019) 312–321
November

Adsorption of Pb^{2+} from aqueous solution by black TiO_{2-x} nanoparticles with enhanced surface area and porosity

Tuqiao Zhang[a], Zhejian Wu[a,b], Rong Chen[a], Qimao Gan[a], Xun Wang[a], Miaomiao Ye[a,*]

[a]*Zhejiang Key Laboratory of Drinking Water Safety and Distribution Technology, College of Civil Engineering and Architecture, Zhejiang University, Hangzhou 310058, China, Tel. +86-571-88206759; Fax: +86-571-88208721; emails: yemiao008@zju.edu.cn (M.M. Ye), ztq@zju.edu.cn (T.Q. Zhang), 3100102002@zju.edu.cn (Z.J. Wu), rongchen@zju.edu.cn (R. Chen), ganqimao@163.com (Q.M. Gan), 21712063@zju.edu.cn (X. Wang)*

[b]*Department of Environment, Yangtze Delta Region Institute of Tsinghua University, Zhejiang, Jiaxing, 314006, China*

Received 6 March 2019; Accepted 22 July 2019

ABSTRACT

TiO_{2-x} nanoparticles with different colours including white, grey, blue grey, light black and black were synthesized via magnesium (Mg) reduction of white Degussa P25 TiO_2 nanoparticles. The as-prepared TiO_{2-x} nanoparticles were used for adsorption of eight metal cations in aqueous solution. Results showed that the TiO_{2-x} nanoparticles with black colour had the best adsorption removal rate for Pb^{2+}. The adsorption kinetic data were fitted with the pseudo-second-order model better than the pseudo-first-order model. The adsorption isotherm was fitted well with both the Langmuir and Freundlich adsorption isotherm. The adsorption capacity of Pb^{2+} by the black TiO_{2-x} nanoparticles at 15°C, 25°C and 35°C were 36.9, 53.4 and 59.2 mg/g, respectively. It was believed that the high adsorption capacity of the black TiO_{2-x} nanoparticles was mainly due to its large surface area, high pore volume, and unique bimodal pore structures. Finally, it was demonstrated that the as-prepared black TiO_{2-x} could be used for adsorption of Pb^{2+} from different natural waters such as tap water, lake water and river water.

Keywords: Adsorption; Black TiO_{2-x}; Langmuir model; Mechanism; Pb^{2+}

1. Introduction

Heavy metal ions are one of the major environmental pollutions in rivers and/or lakes due to their high toxicity and widespread occurrence. Lead (Pb^{2+}) is one of the toxic heavy metal ions which is mainly introduced into the aqueous environment via various industrial products such as batteries, smelting, fuel, paints, etc. [1,2]. Pb^{2+} is a highly toxic substance which can cause a wide range of adverse health consequence for adults and children, particularly damage to the kidneys and immune system even at very low concentration levels [3]. Therefore, the Agency for Toxic Substances and Disease Registry of the United States and the Minister of Health of the People's Republic of China (MOHC) have placed Pb^{2+} on the top of the priority list of toxic pollutants. The maximum permissible limits of Pb^{2+} in drinking water defined by the World Health Organization (WHO) [4], the US Environmental Protection Agency (EPA) standards [5] and the Standards for drinking water quality in China [6] are 0.01, 0.015 and 0.01 mg/L, respectively. Unfortunately, the conventional water treatment processes such as chemical precipitation, coagulation, sedimentation, biodegradation and membrane filtration cannot satisfy with the Pb^{2+} removal [7]. Adsorption process by using novel designed materials has been considered as one of the effective methods for removal of Pb^{2+} from aqueous solution. Recently, organo-functionalized SiO_2-Al_2O_3 [8], CeO_2 nanoparticles supported on $CuFe_2O_4$ nanofibers

* Corresponding author.

[9], polyacrylamide-grafted multiwalled carbon nanotubes [10], Fe–Al–MC nanocomposite [11], poly(ethylenimine) functionalized magnetic nanoparticles [12], and other new materials [13–18] have been successfully prepared for the removal of Pb^{2+}.

Titanium dioxide (TiO_2) is a well-known photocatalyst for its high photocatalytic activity under UV light irradiation. In 2011, Chen et al.'s [19] research group first reported the synthesis of black TiO_{2-x} and its application in water splitting and water purification under visible light irradiation. This discovery triggered the worldwide research interest in utilizing black TiO_{2-x} to enhance the performance of enormous technologies including water splitting, lithium-ion rechargeable batteries, fuel cells, supercapacitors, water purification [20,21]. Up to now, most of the research focus on the removal of heavy metal ions by white TiO_2 [22,23] and modified TiO_2 [24], while no research has been reported on the adsorption removal of heavy metal ions using black TiO_{2-x} as the adsorbent. In this work, TiO_{2-x} nanoparticles with different colours including white, gray, blue gray, light black and black were successfully synthesized by the magnesium (Mg) reduction process. The as-prepared TiO_{2-x} nanoparticles were then used for adsorption of metal cations (M^{n+}) in aqueous solution. The purposes of this study are: (i) to obtain a new absorbent (black TiO_{2-x}) for the removal of Pb^{2+}; (ii) to check the adsorption mechanism of Pb^{2+} by the black TiO_{2-x} nanoparticles.

2. Materials and methods

2.1. Preparation of TiO_{2-x} nanoparticles with different colours

The TiO_{2-x} nanoparticles with different colours were synthesized via an Mg reduction process. Typically, 30, 60, 120, 200 and 400 mg of magnesium powder were mixed with 200 mg of Degussa P25 TiO_2 nanoparticles. The mixtures were first purged with Ar for 15 min and then calcined at 600°C under an Ar atmosphere for 4 h. The cooled mixtures were soaked in 100 mL of HCl (with concentration of 0.5 mol/L) for 4 h, followed by wash with ultrapure water to ensure that there was no Mg residual in TiO_{2-x} nanoparticles. Finally, the TiO_{2-x} samples were dried in vacuum at 60°C for 8 h.

2.2. Batch adsorption and regeneration experiments

The adsorption of eight metal cations (Cr^{3+}, Zn^{2+}, Cu^{2+}, Cd^{2+}, Ni^{2+}, Pb^{2+}, Mn^{2+}, Co^{2+}) by different TiO_{2-x} samples was carried out in 150 mL conical flasks. 100 mL of a stock solution of metal cations (with initial concentration of 0.10 mmol/L) was mixed with different TiO_{2-x} samples, respectively. All batch adsorption processes were conducted at 25°C on an orbital at a shaking speed of 120 rpm and the initial solution pH value of ~4.0. To explore the adsorption isotherms of Pb^{2+}, 100 mL of 0.20, 0.40, 0.60 and 0.80 mmol/L of Pb^{2+} solutions were mixed with 50 mg black TiO_{2-x} respectively. Further demonstration tests were conducted using natural water sources, that is, tap water, lake water and river water for the preparation of Pb^{2+} solution. 1 mol/L of HCl solution was used as the regeneration liquid to examine the recycling performance of the black TiO_{2-x} for removal of Pb^{2+} (initial concentration was 0.80 mmol/L). The adsorbents were dispersed in 20 mL of HCl, and stirred for 4 h for regeneration. The recycled adsorbents were washed with water for several times to remove the remaining protons.

2.3. Analytical methods

The crystalline structures of the TiO_{2-x} nanoparticles were analyzed by powder X-ray diffraction (Bruker D2 Phaser X-ray diffractometer), using Cu Kα radiation at 30 kV. The sizes and morphologies of the TiO_{2-x} nanoparticles were analyzed using a JEOL JEM-1230 transmission electron microscope (TEM) at 120 kV and a FEI Tecnai G2 F20 S TWIN high-resolution transmission electron microscope (HR-TEM) with an accelerating voltage of 200 kV. The surface areas and porosities of the TiO_{2-x} nanoparticles were measured by a N_2 adsorption–desorption measuring instrument (Quantachrome ASIC-2, USA). The elemental compositions on the surface of black TiO_{2-x} before and after adsorption of Pb^{2+} were examined by X-ray photoelectron spectroscopy (XPS, VG ESCALAB Mark II). The concentrations of Pb^{2+} and other cations were determined using an atomic adsorption spectrophotometer model ICE3500 (Thermo Scientific, England) and an inductively coupled plasma mass spectrometry (ICP-MS) model Nexlon 300Q (PE, USA).

3. Results and discussion

3.1. Characterization of TiO_{2-x} with different colours

TiO_{2-x} nanoparticles with different colours were synthesized by Mg reduction of white Degussa P25 TiO_2 nanoparticles. As shown in Fig. 1a, after reacting with 30, 60, 120, 200 and 400 mg of Mg powder, the white P25 TiO_2 powder turned grey, blue grey, light black, black and black, respectively. Here we correspondingly denoted them as Sample 1, Sample 2, Sample 3, Sample 4 and Sample 5. It was reported that the P25 TiO_2 nanoparticles is composed of anatase (~80%) (JCPDS 21-1272) and rutile (~20%) (JCPDS 21-1276) phase [25]. After reduction with 30 mg of Mg, the rutile phase increased and the anatase phase decreased (Fig. 1b). The black TiO_{2-x} nanoparticles (Sample 4 and Sample 5) were composed of TiO_2, Ti_2O and $TiO_{0.89}$.

The sizes and morphologies of the as-synthesized TiO_{2-x} nanoparticles with different colours were examined by TEM and HR-TEM observations, and the results are shown in Fig. 2. The average sizes of the TiO_{2-x} nanoparticles with different colours were all around 25 nm (Figs. 2a–d), which means that the Mg powder reduction process accompanied by HCl wash did not destroy the framework of the TiO_{2-x}. In order to further observe the pore structures of the Sample 3, Sample 4 and Sample 5, the HR-TEM was used. Comparing Sample 4 with Sample 3, (Figs. 2f and g), Sample 4 exhibited much clearer many pore structures with an average pore size of ~3 nm (Figs. 2f and g) can be observed in Sample 4. The formation of the pore structures can be probably explained by the following reasons: The Mg-O-Ti and/or Mg-Ti composites maybe first formed during the Mg reduction of TiO_2, then the Mg atoms were washed away by HCl, resulting in the formation of the voidspore structures. Sample 5 exhibited even larger

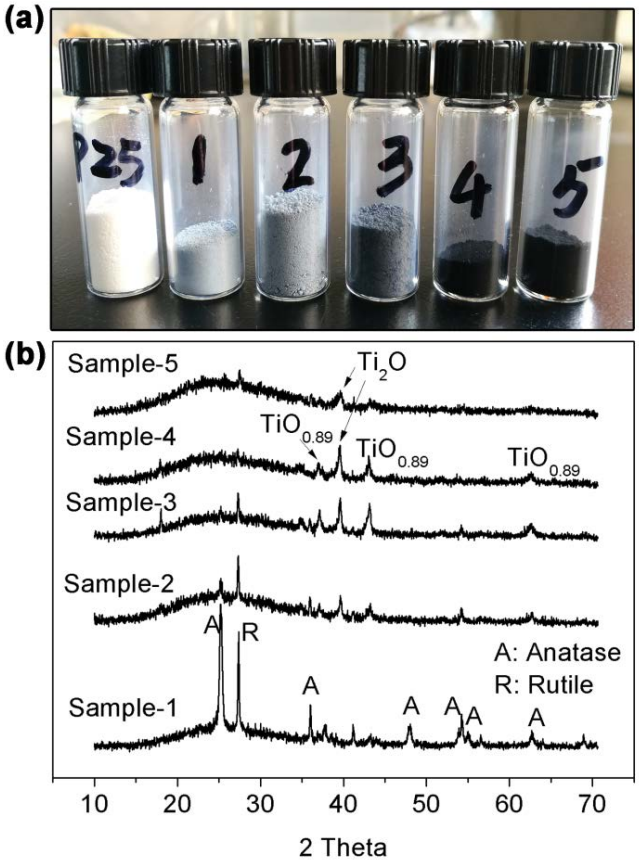

Fig. 1. (a) Digital photos and (b) X-ray diffractions of Sample 1, Sample 2, Sample 3, Sample 4 and Sample 5.

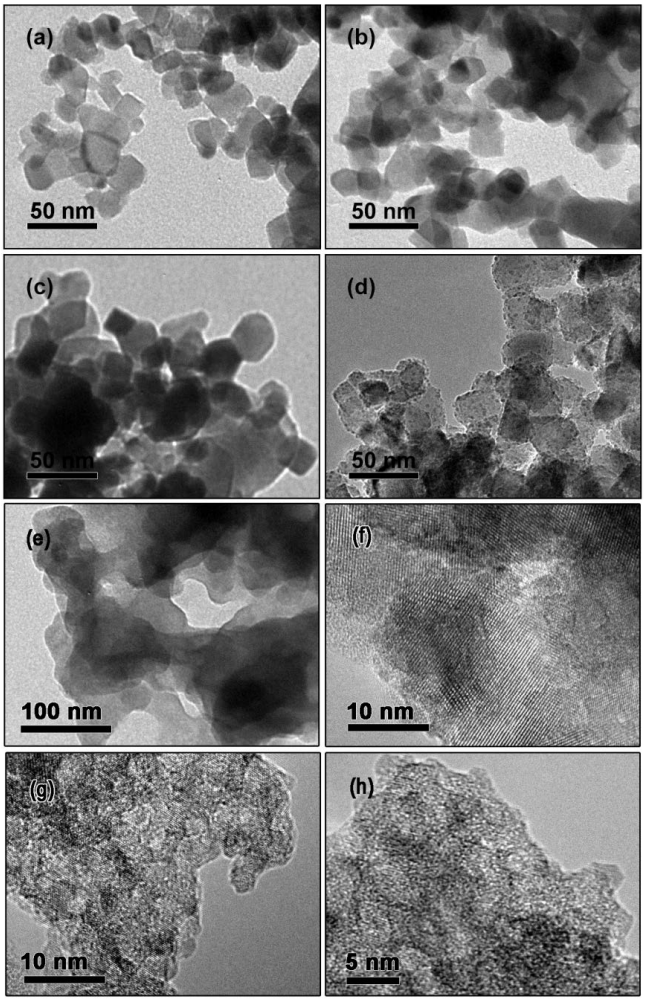

Fig. 2. TEM images of (a) Sample 1, (b) Sample 2, (c) Sample 3, (d) Sample 4, (e) Sample 5, and HR-TEM images of (f) Sample 3 (g) Sample 4, (h) Sample 5.

average pore size compared with Sample 4, which also can be explained by the higher extent of reaction with Mg and the removal of it thereafter.

The detailed pore structures, total pore volumes and the surface areas of the TiO_{2-x} nanoparticles with different colours were further measured by using N_2 adsorption–desorption test, and the results are shown in Fig. 3. For Samples 1, 2 and 3, the adsorption capacity of N_2 decreased with the increasing amount of Mg powder. However, further increasing the Mg dose to 200 mg led to the significantly enhanced N_2 adsorption, which indicates the higher pore volume in agreement with the HR-TEM observation. Furthermore, the adsorption capacity of N_2 decreased again when the Mg dose was further increased to 400 mg (Sample 5 in Fig. 3a). As mentioned above, we believed that too much extent of formation of Mg-O-Ti and/or Mg-Ti composites in turn decreased the number of the formed mesopores because more Mg element were washed away which resulted in the disappearance of the mesopores (as shown in Fig. 3b). In addition, the isotherms of Sample-4 were of the typical type IV pattern with distinct H2 and H3 hysteretic loops in the range of 0.4–0.8 P/P_0 and 0.8–1.0 P/P_0, respectively, indicating the existence of ink-, bottle- and slit-shaped pores according to the IUPAC classification [26]. It is believed that the bimodal pores are beneficial to the enhancement of adsorption performance due to more sites for the adsorption of reactant molecules, faster delivery of various reactants, and fast diffusion of by products [27,28]. Therefore, we believed that the Sample 4 should have the best adsorption activity for heavy metal removal. The corresponding pore size distribution of the TiO_{2-x} samples were determined using the Barrett–Joyner–Halenda (BJH) method from the desorption branch of the isotherms. Data concerning the BET surface areas, and average pore sizes and total pore volumes of the TiO_{2-x} samples with different colours are presented in Table 1.

Besides the surface area and pore structure, the surface charges of the TiO_{2-x} nanoparticles also play an essential role in the adsorption process. Here, the pH value at the point of zero charge (pH_{PZC}) of the TiO_{2-x} nanoparticles was measured by the so-called pH drift method [29], and the results are shown in Fig. 4. The pH_{PZC} values of Sample 1, Sample 4 and Sample 5 were 4.82, 4.16 and 3.02, respectively, showing a gradually decreasing trend with the increasing reduction degree of the TiO_{2-x}. The surface of the TiO_{2-x} nanoparticles will be positively charged when $pH < pH_{PZC}$, and negatively charged when $pH > pH_{PZC}$. As a result, the adsorption efficiency and capacity for Pb^{2+} removal will be significantly

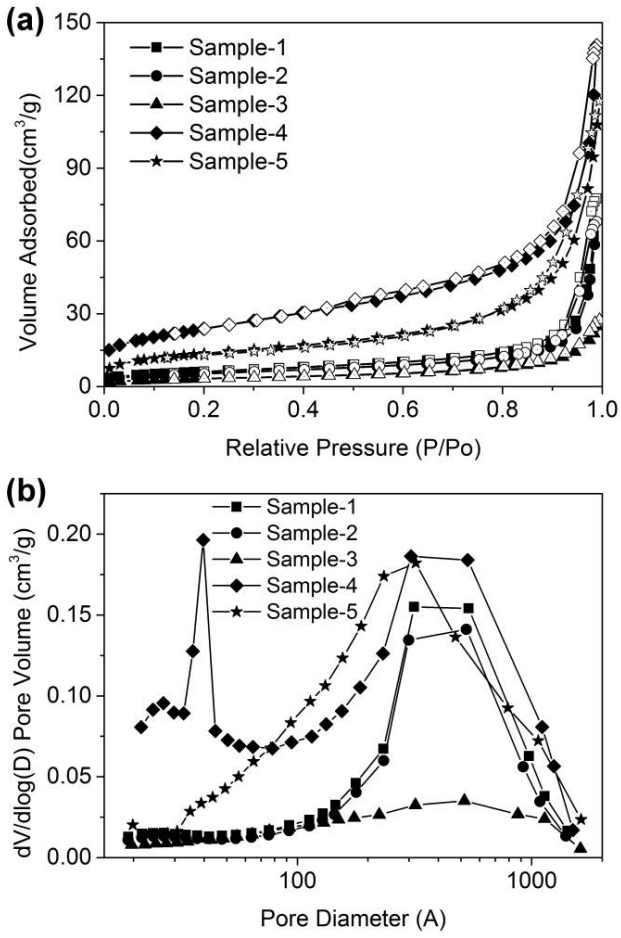

Fig. 3. (a) Nitrogen adsorption–desorption isotherms and (b) BJH pore-size distribution curves of Sample 1, Sample 2, Sample 3, Sample 4 and Sample 5.

Table 1
BET surface areas, average pore sizes and total pore volumes of the different TiO_{2-x} samples

Material	BET surface area (m^2/g)	Average pore size (nm)	Total pore volume (cm^3/g)
P25 [25]	56.5	14.9	0.225
Sample 1	22.4	20.0	0.121
Sample 2	19.5	20.0	0.106
Sample 3	11.8	13.7	0.043
Sample 4	85.6	10.5	0.223
Sample 5	49.0	16.1	0.184

influenced in aqueous solution with different pH values, which will be discussed in the following section.

3.2. Adsorption of eight cations by TiO_{2-x} with different colours

The adsorption of eight metal cations by the TiO_{2-x} with different colours were carried out at room temperature of 25°C, with the initial cation concentration of 0.1 mmol/L,

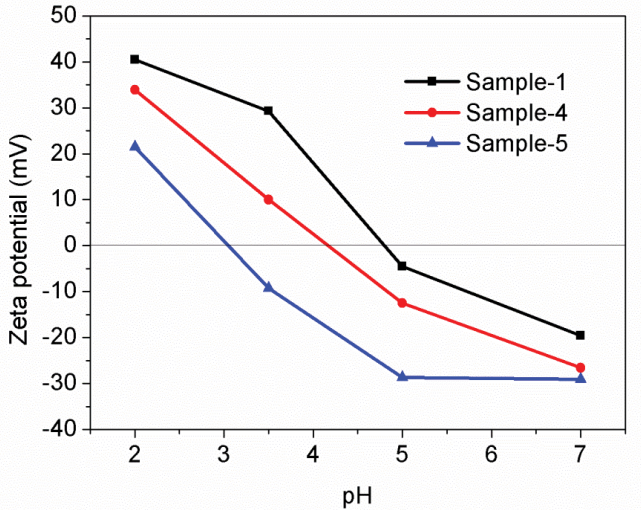

Fig. 4. Zeta potentials of TiO_{2-x} nanoparticles at different pH values.

the TiO_{2-x} dose of 0.5 g/L and the initial solution pH value of ~4.0. The results are shown in Fig. 5a, in which the Cr^{3+} and Pb^{2+} adsorption removal rates by these TiO_{2-x} samples followed the order of Sample 3 < Sample 2 ≈ Sample 1 < P25 < Sample 5 < Sample 4. The order was in agreement with the BET surface areas' order (as shown in Table 1). The adsorption removal rate increased with the increasing surface area, we, therefore, believed that the adsorption was primarily a physical process. Moreover, the Sample 4 possessed the best adsorption activity since it had bimodal pore structures. It has been reported that the bimodal pore structure has a better performance for adsorption [30]. To further explore the adsorption behaviour and mechanism of black TiO_{2-x}, Pb^{2+} was selected as the target pollutant not only because of its highest removal rate in these eight metal cations but also because of its high toxicity and stability in aqueous environment.

3.3. Adsorption of Pb^{2+} by black TiO_{2-x}

The effects of initial Pb^{2+} concentrations on the adsorption removal rates of Pb^{2+} were investigated by varying the initial concentrations of Pb^{2+} ranging from 0.005 to 0.8 mmol/L while keeping other reaction conditions unchanged. At low initial Pb^{2+} concentration of 0.005 mmol/L, the adsorption process quickly achieved equilibrium within 30 min (Fig. 5b). The Pb^{2+} removal rate was up to 99% and the final concentration of Pb^{2+} was less than 10 μg/L, which satisfied the drinking water standard of MOHC [4] (<0.010 mg/L) and USEPA [5] (<0.015 mg/L). However, at a high initial concentration of Pb^{2+}, the adsorption process reached equilibrium within 4 h. The effect of black TiO_{2-x} dose on the Pb^{2+} removal rate was carried out by tuning the TiO_{2-x} dose range from 0.1 to 1.0 g/L and setting the initial concentrations of Pb^{2+} at 0.2 mmol/L and solution pH at 4.0. As shown in Fig. 5c, the Pb^{2+} removal rate was increased with the increasing TiO_{2-x} dose. Finally, the effect of solution pH value on the Pb^{2+} removal rate was also carried out by varying the solution pH values at the range of 3.0–6.9 and setting

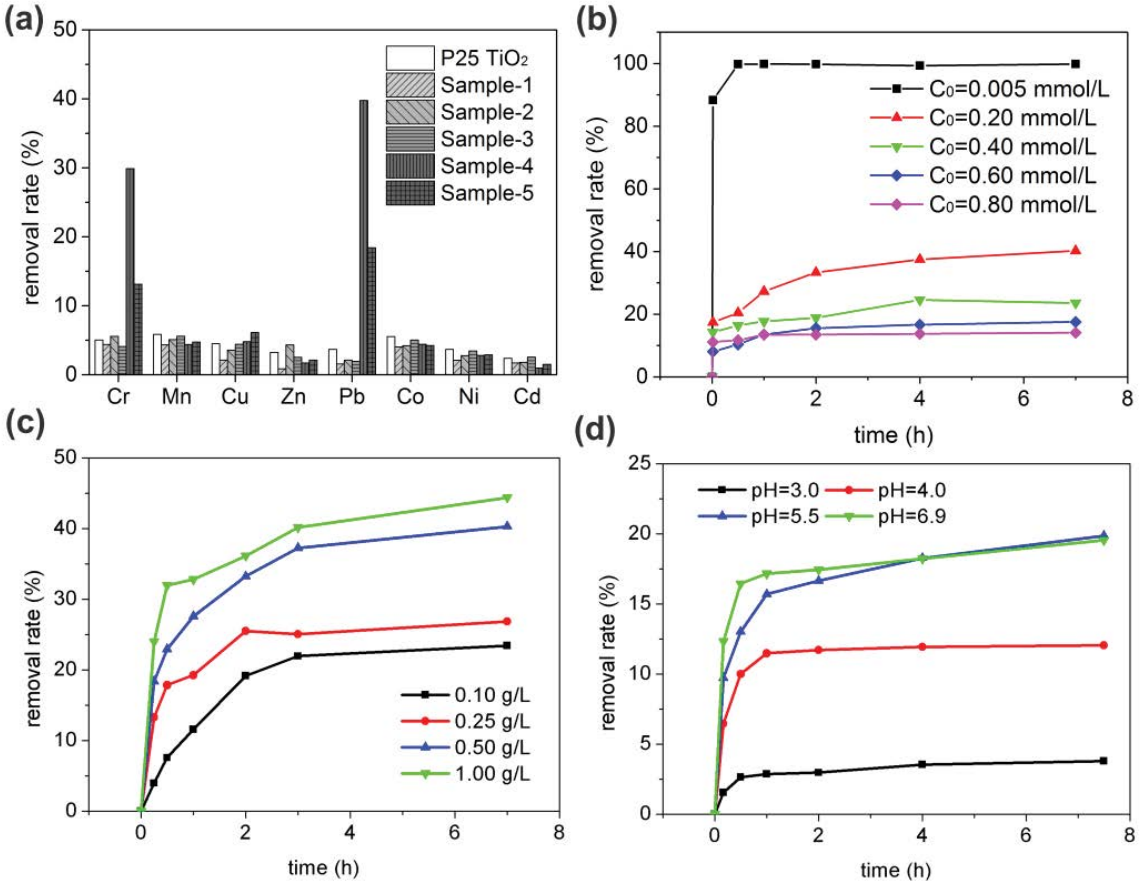

Fig. 5. (a) Adsorption of eight cations by different TiO_{2-x} samples. Effects of (b) initial Pb^{2+} concentration, (c) black TiO_{2-x} dose and (d) solution pH value on the Pb^{2+} removal rates.

the initial concentrations of Pb^{2+} at 0.8 mmol/L and TiO_{2-x} dose at 0.5 g/L. At pH 3.0, the surface of the black TiO_{2-x} was positively charged since its pH_{PZC} was 4.16. The positively charged TiO_{2-x} surface exhibited a dominant electrostatic repulsion against Pb^{2+}, resulting in the low Pb^{2+} removal rate (Fig. 5d). By contrast, the surface of the black TiO_{2-x} was negatively charged when $pH < pH_{PZC}$. As a result, the Pb^{2+} removal rate was significantly enhanced due to the electrostatic attraction [31,32].

3.4. Adsorption kinetics of Pb^{2+} by black TiO_{2-x}

Here, the adsorption processes were fitted by the pseudo-first-order kinetic equations [33] and the pseudo-second-order kinetic equations [34] described as Eqs. (1) and (2), respectively:

$$\ln\left(q_e - q_t\right) = \ln q_e - k_1 t \tag{1}$$

where q_e and q_t are the amounts of the adsorbed Pb^{2+} (mg/g) at equilibrium and at time t (min), respectively. And k_1 is the rate constant of first-order adsorption (min^{-1}).

$$\frac{t}{q_t} = \frac{1}{\left(k_2 q_e^2\right)} + \left(\frac{1}{q_e}\right)t \tag{2}$$

where k_2 is the rate constant of second-order adsorption (g/mg·min). As shown in Figs. 6a and b and Table 2, the adsorption of Pb^{2+} by black TiO_{2-x} fitted well with the pseudo-second-order kinetic model.

3.5. Adsorption isotherms of Pb^{2+} by black TiO_{2-x}

Adsorption isotherm is usually used for describing how adsorbate interacts with adsorbent, and the adsorption capacity of the adsorbent [35]. Langmuir and Freundlich adsorption model are important isotherm models for description many adsorption isotherms. Here, the adsorption isotherms for the removal of Pb^{2+} by black TiO_{2-x} at different reaction temperatures were all modelled by the typical Langmuir and Freundlich adsorption isotherms. The Langmuir isotherm model [36,37] can be expressed as Eq. (3):

$$q_e = \frac{q_m K_L C_e}{\left(1 + K_L C_e\right)} \tag{3}$$

where q_m (mg/g) represents the maximum adsorption capacity of adsorbent and K_L (L/mg) is the Langmuir constant related to the energy of adsorption. q_e (mg/g) and C_e (mg/L) are adsorption capacity and concentration of Pb^{2+} at equilibrium, respectively. The Langmuir isotherm equation can be linearized into Eq. (4):

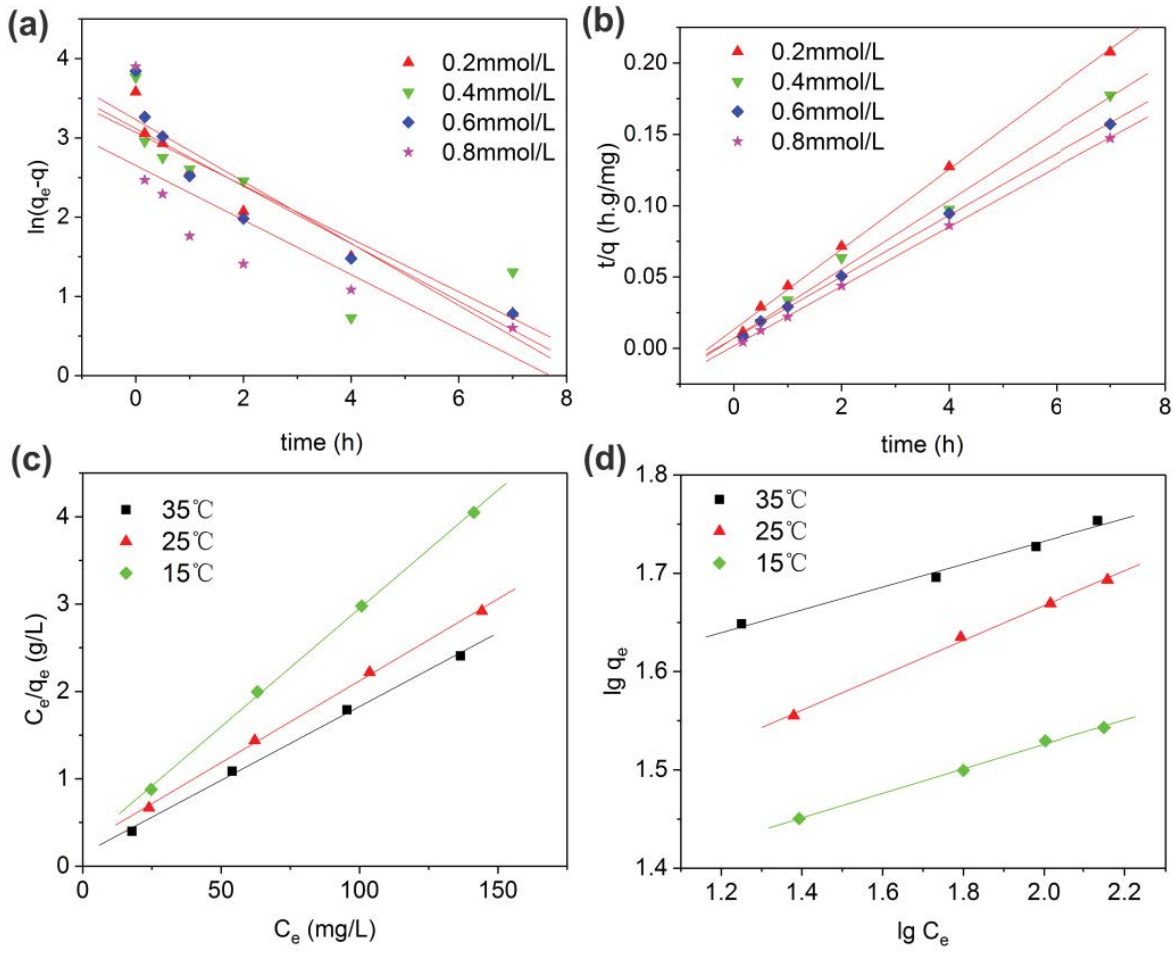

Fig. 6. (a) Adsorption processes of Pb^{2+} by Sample 4 were fitted by (a) the pseudo-first-order kinetic equations and (b) the pseudo-second-order kinetic equations. Linear form of (c) Langmuir isotherm model plots of C_e/q_e vs. C_e and (d) Freundlich isotherm model plots of log q_e vs. log C_e at 15°C, 25°C, 35°C respectively.

Table 2
Adsorption kinetics of Pb^{2+} by black TiO_{2-x} fitted with the pseudo-first-order kinetics and pseudo-second-order kinetics

Kinetic model	Initial concentration (mmol/L)	Parameters			
		Experimental q_e (mg/g)	Predicted q_e (mg/g)	k_1 (h^{-1})	R^2
Pseudo-first order	0.20	35.9	22.6	0.363	0.910
	0.40	43.2	21.5	0.335	0.645
	0.60	46.7	25.3	0.391	0.856
	0.80	49.4	13.0	0.334	0.517
		Experimental q_e (mg/g)	Predicted q_e (mg/g)	k_2 (g/mg h)	R^2
Pseudo-second order	0.20	35.9	35.6	0.0597	0.997
	0.40	43.2	41.4	0.0814	0.992
	0.60	46.7	46.3	0.0663	0.999
	0.80	49.4	47.9	0.2549	0.999

$$\frac{C_e}{q_e} = \frac{C_e}{q_m} + \frac{1}{K_L q_m} \quad (4)$$

In order to calculate the maximum adsorption capacity, equilibrium data were analyzed by the linear form. The different parameters of Langmuir isotherm were determined from the slope and intercept of plot C_e/q_e vs. C_e at 15°C, 25°C, 35°C, respectively. Fig. 6c shows the adsorption process well-fitted Langmuir adsorption isotherm with all correlation coefficient values >0.995. The maximum adsorption capacities (q_m) of Pb^{2+} by black TiO_{2-x} were 36.9, 53.4 and 59.2 mg/g at 15°C, 25°C and 35°C, respectively (Table 3). The comparison of q_m of other adsorbents for the removal of Pb^{2+} is presented in Table 4. The q_m value was higher than that of most of the reported adsorbents, which indicates that the black TiO_{2-x} was a suitable adsorbent for the removal of Pb^{2+} from aqueous solution. In addition, the adsorption capacity increased with the increasing temperature, indicating that the adsorption process of Pb^{2+} by black TiO_{2-x} was an endothermic process.

By contrast, Freundlich adsorption isotherm was also used for fitting the adsorption experimental data. The original Freundlich equation and its linear form can be expressed as Eq. (5) [38] and Eq. (6), respectively [36]:

$$q_e = K_F C_e^{1/n} \quad (5)$$

$$\log q_e = \log K_F + \frac{1}{n(\log C_e)} \quad (6)$$

where K_F represents the Freundlich adsorption capacity and n is the term used for the heterogeneity factor related to adsorption intensity. The parameters of Freundlich isotherm model were calculated by the plot of log q_e vs. log C_e (Fig. 6d and Table 3). It can be seen from Table 3 that the adsorption isotherms for the removal of Pb^{2+} by black TiO_{2-x} at different reaction temperatures were also well fitted by the Freundlich model. The K_F and n were found as 18.9, 20.5 and 31.6 mg/g, and 8.0, 5.6 and 8.6 at 15°C, 25°C and 35°C, respectively.

3.6. Recycling

The recycling is very important for evaluation of the adsorption ability. Recycling test was carried out using 1 mol/L of HCl solution as the regeneration eluent, because the adsorbed Pb^{2+} can be desorbed under highly acidic condition, which was explained in the above section about pH effect. Fig. 7 shows the result of five cycles of adsorption–regeneration test. After the first regeneration cycle by HCl, 85.3% of adsorption sites of the black TiO_{2-x} could be regenerated, and 39.5 mg/g of Pb^{2+} was re-adsorbed. After five cycles, the adsorption capacity for Pb^{2+} removal by black TiO_{2-x} was reduced to 31.7 mg/g. The decreased adsorption capacity

Table 3
Adsorption isotherms for the removal of Pb^{2+} by black TiO_{2-x} modelled by the Freundlich and Langmuir adsorption isotherms

Temperature °C	Langmuir isotherm model			Freundlich isotherm model		
	q_m (mg/g)	K_L (L/mg)	R^2	K_F (mg/g)	n	R^2
15	36.9	0.0757	0.999	18.9	8.0	0.996
25	53.4	0.112	0.998	20.5	5.6	0.996
35	59.2	0.122	0.996	31.6	8.6	0.980

Table 4
The maximum adsorption capacities (q_m) of Pb^{2+} by different adsorbents

Number	Adsorbent	q_m mg/g	Reference
1	Titanate whiskers	384.6	[1]
2	Coffee grounds and attapulgite clay (CG/AC)	4.45	[2]
3	APTES-modified hollow TiO_2 nanospheres	7.13	[7]
4	$CeO_2/CuFe_2O_4$ nanofibers	972.4	[9]
5	Fe–Al–MC nanocomposite	40.0	[11]
6	Poly(ethylenimine) functionalized magnetic nanoparticles	46	[12]
7	Fe_3O_4@UiO-66-NH_2 core/shell nanocomposite	19.8	[13]
8	Allylamine and N,N-dimethylacrylamide modified glass nanoparticles	26.7	[14]
9	Canola stalk	10.9	[15]
10	*Sargassum cinereum* (macroalgae) biomass	21.6	[16]
11	Iron ore tailing with phosphorus	17.0	[17]
12	Bentonite–biochar nanocomposite	44.7	[18]
13	Black TiO_{2-x}	53.4	our work

was mainly due to the incomplete desorption of Pb^{2+} during the HCl regeneration process.

3.7. Possible adsorption mechanism

As mentioned above, we believed that the adsorption process was primarily a physical process since the adsorption capacity increased with the increasing surface area. To further explore if there was any formation of chemical bonds during the adsorption process, the XPS of the black TiO_{2-x} before and after adsorption of Pb^{2+} were examined, and the result is shown in Fig. 8. The appearance of a new Pb 4f 7/2 peak at 138.3 eV (Fig. 8a) suggested the successful adsorption of Pb^{2+} on the black TiO_{2-x}. The Ti2p 3/2 peak at 457.9 eV (Fig. 8b) and O 1s peak at 529.5 eV (Fig. 8c) before and after adsorption of Pb^{2+} did not shift, indicating that no new chemical bonds between Ti, O and other elements were formed during the adsorption process. Therefore, we believed that the adsorption process of Pb^{2+} by black TiO_{2-x} was only a physical process. A possible adsorption mechanism of Pb^{2+} by the black TiO_{2-x} is presented in Fig. 9.

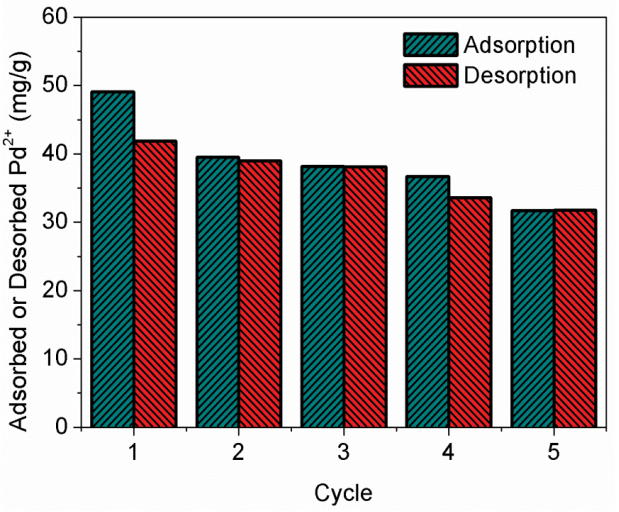

Fig. 7. Recycling performance of black TiO_{2-x} in five cycles.

3.8. Adsorption of Pb^{2+} from natural water

To explore the potential application of the black TiO_{2-x} nanoparticles for removal of Pb^{2+} in natural water source, tap water, lake water and river water were used as the background water to prepare Pb^{2+} solution. The initial Pb^{2+} concentration in this experiment was 0.005 mmol/L. The water quality parameters and the removal rates of the Pb^{2+} in these three natural waters are shown in Table 5. The removal rates of Pb^{2+} in tap water, lake water and river

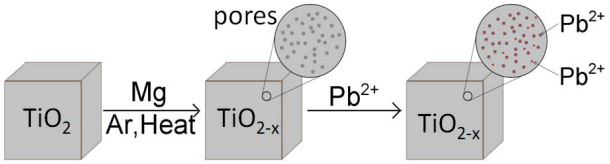

Fig. 9. Possible adsorption mechanism of Pb^{2+} by the black TiO_{2-x}.

Table 5
Water quality parameters of three natural water and the Pb^{2+} removal rates

Natural water	Turbidity NTU	pH	TOC mg/L	Cl^- mg/L	NO_3^- mg/L	SO_4^{2-} mg/L	Na^+ mg/L	Ca^{2+} mg/L	R_3 (%)	R_6 (%)
West lake	11.0	7.16	4.14	17.3	10.7	23.8	17.3	101.0	88.0	98.8
Qiantang river	14.4	7.02	3.96	15.4	7.52	22.9	19.1	12.8	86.0	98.2
Tap water	0.05	6.85	–	18.2	9.30	16.2	17.0	71.2	96.6	99.4

R_3: Removal rate at 3 h; R_6: Removal rate at 6 h.
Black TiO_{2-x} dose: 0.5 g/L, initial Pb^{2+} concentration: 0.005 mmol/L, solution volume: 100 mL, adsorption temperature: 25°C.

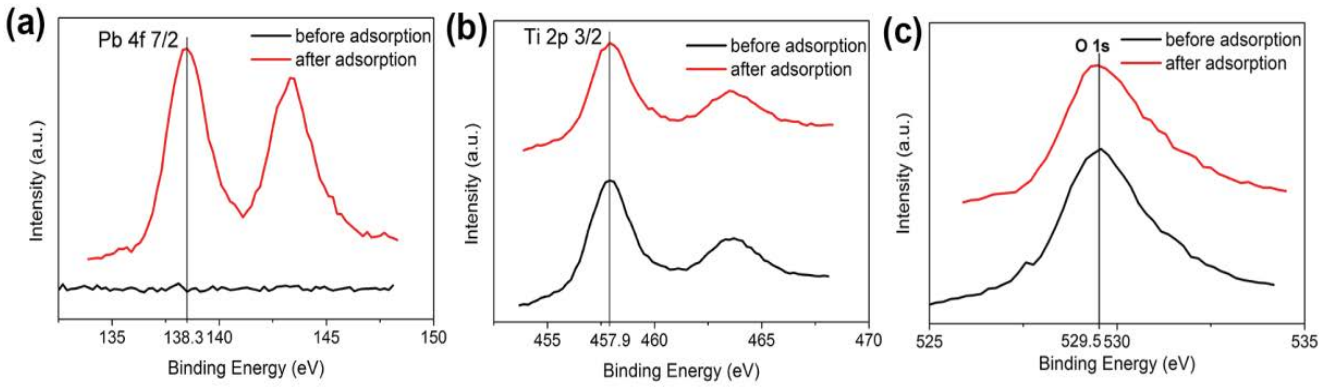

Fig. 8. High-resolution XPS spectra of (a) Pb 4f; (b) Ti 2p 3/2; (c) O1s region from the surface of the black TiO_{2-x} before and after Pb^{2+} adsorption.

water were 98.8%, 98.2% and 99.4% at the adsorption time of 6 h, respectively. Compared with pure water, no Pb^{2+} removal rate was lost, indicating that the as-prepared black TiO_{2-x} nanoparticles can be used for adsorption of Pb^{2+} from natural water.

4. Conclusions

In summary, TiO_{2-x} nanoparticles with different colours were successfully synthesized by Mg powder reduction with Degussa P25 TiO_2 nanoparticles. The surface areas, total pore volumes of the as-prepared TiO_{2-x} samples first decreased with the increasing addition of Mg powder, then suddenly increased to 85.6 m^2/g and 0.223 cm^3/g, respectively, with further addition of Mg power. However, too much addition of Mg power also led to the decreased surface areas and total pore volumes. The black TiO_{2-x} (Sample 4) possessed the best adsorption activity for metal cations removal not only because of its high surface area and total pore volume but also because of its unique bimodal pore structures. The adsorption isotherm for the removal of Pb^{2+} by black TiO_{2-x} nanoparticles could be fitted well with the Langmuir model. The adsorption capacity of Pb^{2+} by the black TiO_{2-x} nanoparticles at 15°C, 25°C and 35°C were 36.9, 53.4 and 59.2 mg/g, respectively. Finally, it was believed that this black TiO_{2-x} was a great potential adsorbent for the removal of Pb^{2+} ions from aquatic environments.

Acknowledgements

The present work was financially supported by the Funds for International Cooperation and Exchange of the National Natural Science Foundation of China (No. 51761145022), the Public Welfare Technology Application Research Project of Zhejiang Province (No. LGG18E080002), the National Science and Technology Major Protects for Water Pollution Control and Treatment (No. 2017ZX07201004), and the Fundamental Research Funds for the Central Universities (No. 2018FZA4017).

Symbols

q_e — Adsorption capacity of Pb^{2+} at equilibrium, mg/g
q_t — Adsorption capacity of Pb^{2+} at time t, mg/g
k_1 — Rate constant of first-order adsorption, min^{-1}
k_2 — Rate constant of second-order adsorption, g/mg min
q_m — Maximum adsorption capacity of adsorbent, mg/g
C_e — Concentration of Pb^{2+} at equilibrium, mg/L
K_L — Langmuir constant related to the free energy of adsorption, L/mg
K_F — Freundlich adsorption capacity
n — Heterogeneity factor related to adsorption intensity.
Sample 1 — 30 mg of Mg powder reacts with 200 mg of P25 TiO_2
Sample 2 — 60 mg of Mg powder reacts with 200 mg of P25 TiO_2
Sample 3 — 120 mg of Mg powder reacts with 200 mg of P25 TiO_2
Sample 4 — 200 mg of Mg powder reacts with 200 mg of P25 TiO_2
Sample 5 — 400 mg of Mg powder reacts with 200 mg of P25 TiO_2

References

[1] Y. Hang, H.B. Yin, A.L. Wang, L.Q. Shen, Y.H. Feng, R.J. Liu, Preparation of titanate whiskers starting from metatitanic acid and their adsorption performances for Cu(II), Pb(II), and Cr(III) ions, Water Air Soil Pollut., 225 (2014) 2095.
[2] L. Liu, L.J. Yu, W. Zhang, J.H. Fan, Q.T. Zuo, M.J. Li, Z.F. Yan, Z.C. You, R.Y. Wang, Adsorption performance of Pb(II) ions from aqueous solution onto a novel complex of coffee grounds and attapulgite clay, Desal. Wat. Treat., 153 (2019) 208–215.
[3] S.V. Hosseini, S. Sobhanardakani, R. Tahergorabi, P. Delfieh, Selected heavy metals analysis of persian sturgeon's (*Acipenser persicus*) caviar from southern caspian sea, Biol. Trace Elem. Res., 154 (2013) 357–362.
[4] Guidelines for Drinking-water Quality, 4th ed., World Health Organization, 2011. Available at: http://apps.who.int/iris/bitstream/10665/44584/1/9789241548151_eng.pdf.
[5] 2012 Edition of the Drinking Water Standards and Health Advisories, Office of Water, US Environmental Protection Agency. Available at: https://www.epa.gov/ground-water-and-drinking-water/table-regulated-drinking-water-contaminants.
[6] The Chinese National Standards for Drinking Water Quality (GB 5749-2006), 2006. Available at: http://www.nhfpc.gov.cn/cmsresources/zwgkzt/wsbz/new/20070628143525.pdf.
[7] Y. Hang, H.B. Yin, Y.Q. Ji, Y. Liu, Z.P. Lu, A.L. Wang, L.Q. Shen, H.X. Yin, Adsorption performances of naked and 3-aminopropyl triethoxysilane-modified mesoporous TiO_2 hollow nanospheres for Cu^{2+}, Cd^{2+}, Pb^{2+}, and Cr(VI) Ions, J. Nanosci. Nanotechnol., 17 (2017) 5539–5549.
[8] M.B. Jazi, M. Arshadi, M.J. Amiri, A. Gil, Kinetic and thermodynamic investigations of Pb(II) and Cd(II) adsorption on nanoscale organo-functionalized SiO_2-Al_2O_3, J. Colloid Interface Sci., 422 (2014) 16–24.
[9] F. Talebzadeh, R. Zandipak, S. Sobhanardakani, CeO_2 nanoparticles supported on $CuFe_2O_4$ nanofibers as novel adsorbent for removal of Pb(II), Ni(II), and V(V) ions from petrochemical wastewater, Desal. Wat. Treat., 57 (2016) 28363–28377.
[10] S. Yang, J. Hu, C. Chen, D. Shao, X. Wang, Mutual effects of Pb(II) and humic acid adsorption on multiwalled carbon nanotubes/polyacrylamide composites from aqueous solutions, Environ. Sci. Technol., 45 (2011) 3621–3627.
[11] H. Tsade, B. Abebe, H.C.A. Murthy, Nano sized Fe-Al oxide mixed with natural maize cob sorbent for lead remediation, Mater. Res. Express, 6 (2019) 085043.
[12] P.B. Rathod, S. Chappa, K.S.A. Kumar, A.K. Pandey, A.A. Athawale, Poly(ethylenimine) functionalized magnetic nanoparticles for sorption of Pb, Cu, and Ni: potential application in catalysis, Sep. Sci. Technol., 54 (2019) 1588–1598.
[13] S. Feng, S.G. Liu, S.S. Feng, R.B. Wang, Efficient removal of Pb^{2+} from water using Fe_3O_4@UiO-66-NH_2 core/shell nanocomposite, Desal. Wat. Treat., 151 (2019) 251–263.
[14] S. Arjmandpour, H.A. Panahi, Removal of lead ion from environmental samples using modified glass nanoparticles, Desal. Wat. Treat., 137 (2019) 212–220.
[15] H. Hashtroudi, M. Khiadani, G.Z. Sun, Pb(II) ions sequestration from aqueous solutions by canola stalk: isotherms and kinetics studies, Desal. Wat. Treat., 118 (2018) 205–215.
[16] K.K. Kumar, M.K. Prasad, G. Baburao, M. Sudhakar, J. Sivajyothi, T. Sathish, C.V.R. Murthy, A fortunate marine algae biomass, *Sargassum cinereum* for removal of Pb(II): studies on thermodynamics, kinetics and characterization, Desal. Wat. Treat., 116 (2018) 179–186.
[17] X.L. Yuan, W.T. Xia, J. An, X.J. Zhou, X.Y. Xiang, J.G. Yin, W.Q. Yang, Adsorption characteristics of Pb(II) ions onto wasted iron ore tailing with phosphorus used as natural adsorbent from aqueous solution, Desal. Wat. Treat., 98 (2017) 222–232.

[18] F.E. Setaredjo, Y.H. Ju, S. Ismadji, A. Ayucitra, Removal of Cu(II) and Pb(II) from wastewater using biochar-clay nanocomposite, Desal. Wat. Treat., 82 (2017) 188–200.
[19] X. Chen, L. Liu, P.Y. Yu, S.S. Mao, Increasing solar absorption for photocatalysis with black hydrogenated titanium dioxide nanocrystals, Science, 331 (2011) 746–750.
[20] X. Chen, L. Liu, F. Huang, Black titanium dioxide (TiO_2) nanomaterials, Chem. Soc. Rev., 44 (2015) 1861–1885.
[21] T. Lin, C. Yang, Z. Wang, H. Yin, X. Lü, F. Huang, J. Lin, X. Xie, M. Jiang, Effective nonmetal incorporation in black titania with enhanced solar energy utilization, Energy Environ. Sci., 7 (2014) 967–972.
[22] L.B. Khalil, W.E. Mourad, M.W. Rophael, Photocatalytic reduction of environmental pollutant Cr(VI) over some semiconductors under UV/visible light illumination, Appl. Catal., B, 17 (1998) 267–273.
[23] L. Yu, X. Peng, F. Ni, J. Li, D. Wang, Z. Luan, Arsenite removal from aqueous solutions by γ-Fe_2O_3-TiO_2 magnetic nanoparticles through simultaneous photocatalytic oxidation and adsorption, J. Hazard. Mater., 246 (2013) 10–17.
[24] J.K. Yang, S.M. Lee, Removal of Cr(VI) and humic acid by using TiO_2 photocatalysis, Chemosphere, 63 (2006) 1677–1684.
[25] M. Ye, Z. Chen, W. Wang, J. Shen, J. Ma, Hydrothermal synthesis of TiO_2 hollow microspheres for the photocatalytic degradation of 4-chloronitrobenzene, J. Hazard. Mater., 184 (2010) 612–619.
[26] M. Thommes, K. Kaneko, A.V. Neimark, J.P. Olivier, F. Rodriguez-Reinoso, J. Rouquerol, K.S.W. Sing, Physisorption of gases, with special reference to the evaluation of surface area and pore size distribution, Pure Appl. Chem., 87 (2015) 1051–1069.
[27] Y. Chen, D.D. Dionysiou, A comparative study on physicochemical properties and photocatalytic behavior of macroporous TiO_2-P25 composite films and macroporous TiO_2 films coated on stainless steel substrate, Appl. Catal., A, 317 (2007) 129–137.
[28] Y. Chen, D.D. Dionysiou, Bimodal mesoporous TiO_2–P25 composite thick films with high photocatalytic activity and improved structural integrity, Appl. Catal., B, 80 (2008) 147–155.
[29] M.M. Ye, Z.L. Chen, T.Q. Zhang, W.Y. Shao, Effect of calcination temperature on the catalytic activity of nanosized TiO_2 for ozonation of trace 4-chloronitrobenzene, Water Sci. Technol., 66 (2012) 479–486.
[30] J.C. Groen, J. Pérez-RamíRez, Critical appraisal of mesopore characterization by adsorption analysis, Appl. Catal., A, 268 (2004) 121–125.
[31] S. Sobhanardakani, R. Zandipak, Synthesis and application of TiO_2/SiO_2/Fe_3O_4 nanoparticles as novel adsorbent for removal of Cd(II), Hg(II) and Ni(II) ions from water samples, Clean Technol. Environ. Policy, 19 (2017) 1913–1925.
[32] S. Sobhanardakania, A. Jafarib, R. Zandipaka, A. Meidanchic, Removal of heavy metal (Hg(II) and Cr(VI)) ions from aqueous solutions using Fe_2O_3@SiO_2 thin films as a novel adsorbent, Process Saf. Environ., 120 (2018) 348–357.
[33] Y.S. Ho, G. Mckay, Sorption of dye from aqueous solution by peat, Chem. Eng. J., 70 (1998) 115–124.
[34] Y.S. Ho, G. Mckay, The kinetics of sorption of divalent metal ions onto sphagnum moss peat, Water Res., 34 (2000) 735–742.
[35] C. Namasivayam, Removal and recovery of molybdenum from aqueous solutions by adsorption onto surfactant-modified coir pith, a lignocellulosic polymer, Clean Soil Air Water, 37 (2009) 60–66.
[36] J. Febrianto, A.N. Kosasih, J. Sunarso, Y.H. Ju, N. Indraswati, S. Ismadji, Equilibrium and kinetic studies in adsorption of heavy metals using biosorbent: a summary of recent studies, J. Hazard. Mater., 162 (2009) 616–645.
[37] I. Langmuir, The adsorption of gases on plane surfaces of glass, mica and platinum, J. Chem. Phys., 40 (1918) 1361–1403.
[38] H. Freundlich, Über die adsorption in lösungen, Zeitschrift für Physikalische Chemie, J. Am. Chem. Soc., 57 (1906) 121–125.